



Structural Features, Superatomic Properties, and Adsorptions of Zn–Cd Nanoalloy

Ying Meng¹ · Qiman Liu¹ · Longjiu Cheng²

Received: 19 March 2023 / Accepted: 3 July 2023 / Published online: 14 July 2023
© The Author(s), under exclusive licence to Springer Science+Business Media, LLC, part of Springer Nature 2023

Abstract

Zn–Cd alloys are important industrial materials which have attracted much attentions in recent years. But, few reports on Zn–Cd clusters are currently available. An interesting structural feature in previous studies is that Zn and Cd atoms do not mix in binary Zn–Cd clusters. However, the analysis based on the empirical potential function can only give very limited structure information about them. Here, geometric structures of $(\text{Zn–Cd})_n$ ($n = 1–9$) clusters are globally searched by the unbiasedly genetic algorithm with DFT methods. We found that the ground state structures of Zn–Cd clusters are singlet states and prefer compact characteristics, where the Cd atoms prefer to be located on the surfaces of the structures, thus coating Zn atoms that are for the kernel growths. The E_b and Δ_2E results show that the $(\text{Zn–Cd})_2$ and $(\text{Zn–Cd})_5$ clusters have higher stability than that of their neighbors. The molecular dynamics simulations verify that they still have excellent thermal stability at 700 K. The molecular orbitals and DOS reveal that the 8/20 valence electrons of the $(\text{Zn–Cd})_2$ and $(\text{Zn–Cd})_5$ clusters fill the superatomic shells resulting in electronic configurations of $1S^21P^6/1S^21P^61D^{10}2S^2$, respectively. Moreover, we considered different adsorption structures of $(\text{Zn–Cd})_2$ with one CO molecule, and only the four stable isomers are finally obtained. It is found that the CO in the form of molecule is adsorbed on the cluster, resulting in the unbroken C–O bond.

Keywords Zn–Cd clusters · Geometry features · Stability · Electronic structures

Introduction

Zinc and Cadmium are known alloying metal elements with the atomic size differences of less than 10%, which are both divalent and have small electronegativity differences, leading to a widespread application of alloy properties in the fields of superconductor and semiconductor, as well as surface coating and plating processes materials [1–6]. These alloying elements are used for soldering processes since many solders may contain Cd because of its low melting point, and brazing processes for higher temperatures should

use alloys containing large amounts of Zn [7–9]. Furthermore, Zn–Cd alloys are simple eutectic systems and can be regarded as appropriate models to comprehend the formations and mechanical properties of composite materials, because of their regular lamellar structures [10, 11]. The calculated local ordering energies explain successfully the existence of a short-range order in the insolubility between Cd and Zn [12]. For instance, Zinc alloys containing 0.1% Cadmium have been reported to improve the mechanical properties of rolled, drawn or extruded Zinc, and such alloys containing Cadmium in the range 0.025 to 0.15% are used as sacrificial anodes in the corrosion protection of structural steelwork immersed in seawater [13–15].

The studies of Zn–Cd alloy materials focused on mechanical effects, structure surfaces and configurationally thermodynamic properties. For example, Fornaro et al. used metallographic analysis of the samples to evaluate aspects of the microstructure details of Zn–Cd alloys during the planar to cellular transition and extended the classical interpretation of morphological stability approach in order to interpret the experimental results [16]. The compositions and temperature dependences of the thermal and

✉ Qiman Liu
qimliu@ustc.edu.cn

✉ Longjiu Cheng
clj@ustc.edu.cn

¹ School of Chemistry and Materials Engineering,
Huainan Normal University, Huainan 232000,
People's Republic of China

² Key Laboratory of Structure and Functional Regulation
of Hybrid Materials, Anhui University, Hefei 230000,
People's Republic of China

electrical conductivities of three different Cd–Zn alloys were studied in the temperature range of 300–650 K [17]. Koirala et al. investigated the configurations and thermodynamic properties of molten Zn–Cd alloys at 800 K, and the results showed that the Cadmium atoms are apt to segregate on surfaces of the molten alloys while Zinc atoms maintain mainly in the bulk [18]. Recently, Shrestha et al. investigated the structural behaviors of Cd–Zn alloys at molten state by computing thermodynamic functions and structural functions, and they found that Cd–Zn alloys are segregating and weakly interacting in nature [19].

Although the importance of the Zn–Cd alloys is self-evident, the information about these systems at the atomistic level is comparatively scarce and rarely available. As everyone knows, macroscopic properties of industrial alloys are closely related to their nanostructures, and the formations of microstructures resulting from crystal growths first need to be understood at atomic levels [20–24]. Microstructures of alloys are crucial for understanding understanding the first stage of growth mechanisms, and it would be valuable to establish connections between the observed nanostructure features and corresponding macroscopic properties [25–27]. Unfortunately, there are only few reports of the Zn–Cd clusters currently available through the Google Scholar. Amirouche et al. reported structural features and energetics of Zn–Cd clusters up to 4 atoms, which were modeled with an empirical many-body potential energy function based on experimental data [28]. Subsequently, they employed the same empirical potential to carry out molecular dynamics calculations on either small (up to 8 atoms) and larger Zn–Cd clusters with 50 atoms [29]. Based on these, Marques et al. used the evolutionary algorithm with the Gupta potential to study the growing patterns of Zn–Cd clusters with equal Zn and Cd compositions [10]. An interesting structural feature obtained by the empirical function in reported works is that Zn and Cd atoms do not mix in binary Zn–Cd clusters. However, it is well known that the analysis based on the empirical potential functions can only give very limited structure information about Zn–Cd clusters, and cannot be used to analyze the electronic properties.

The electronic and structural stability of metal clusters can be described to the superatom model, which is based on the electronic shell filling rule [30]. When metal clusters have a certain number of valence electrons, these electrons are confined in a jellium-like potential field, and they occupy a series of quantized orbitals, including 1S, 1P, 1D, 2S, 1F, 2P, and so on, in order of increasing energy. These superatomic orbitals are different from atomic orbitals and have unique electronic properties. This theory of superatom has achieved great success in discussing the electronic structures of spherical metal clusters [31, 32]. For example, the icosahedral Al_{13} , as it is known, requires an extra electron to close the $2P^6$ shell and thus behaves like a halogen atom [33].

Here, geometric structures of $(Zn-Cd)_n$ ($n = 1-9$) clusters are globally searched by using the unbiasedly genetic algorithm (GA) with DFT methods. The configuration features, stability and electronic structures of them are emphatically analyzed. The behaviors of Zn–Cd clusters conformations on the finite temperatures are also explored. Moreover, the valence electron fillings, superatom and adsorption properties of these series are given in detail by molecular orbitals, the density of states and NPA charges.

Computational Methods and Details

The low-lying isomers of $(Zn-Cd)_n$ ($n = 1-9$) clusters are globally searched and located by using the GA-DFT methods. The GA algorithm belong to a type of search heuristic algorithms that simulated evolution processes to create inheritance, mutation, selection, and crossover schemes for optimization problems [34–37]. Such strategy has been widely used to predict configurations of alloy clusters [34, 38–40]. In the GA-DFT procedures, conformations of alloy clusters at the PBE0/Def2-SV level are unbiasedly scanned on their potential energy surfaces, and the purpose of using this basis set is to save time. The spin multiplicity of per isomer is initially set to 1 (with even valence electrons). During the optimization procedures of each component, more than 1000 samples are calculated using the DFT method. After global optimizations, all obtained isomers of $(Zn-Cd)_n$ ($n = 1-9$) sorted by energies are re-optimized at a higher PBE0/Def2-SVP theoretical level [41, 42], and spin multiplicities are reset to 1, 3, and 5 to find the global minima (GM) structures. The quality of self-consistent field (SCF) convergence tolerance is set with a convergence criterion of 1×10^{-6} hartree on total energy and electron density, 2×10^{-3} hartree \AA^{-1} on the gradient, and 5×10^{-3} \AA on the displacement in our calculations. All first-principles calculations are based on the Gaussian 09 package [43]. Molecular visualization is performed using MOLEKEL 5.4 [44]. Furthermore, the density of states (DOS) calculations are performed in the Multiwfn program package [45].

The ab initio molecular dynamics simulations (AIMD) are carried out in the Vienna ab initio simulation package (VASP) [46]. The projector-augmented plane wave (PAW) approach is used to describe the ion-electron interactions. The PBE functional and a 450 eV cutoff for the plane-wave basis set are adopted. The convergence threshold is set to 10^{-4} eV in energy and 0.01 eV \AA^{-1} in force. We select the Nose–Hoover method to control AIMD temperatures [47].

Results and Discussions

The Structure Characters of Optimized (Zn–Cd)_n (n = 1–9) Clusters

As we well know, Zn is the fourth period group-IIB element, and Cd is the fifth period group-IIB element. Zinc and Cadmium are the atomic size differences of less than 10%, and they are both divalent and have small electronegativity differences. The GM structures for (Zn–Cd)_n (n = 1–9) with 1:1 stoichiometric ratio of Zn and Cd are first searched at the PBE0/Def2-SVP level by using the GA algorithm combined with DFT methods. This functional and the basis set with relativistic effects are widely used in metal clusters and confirmed to be credible. Table 1 presents the benchmark calculation results for DFT/Def2SVP and CCSD(T)/Def2TZVP. The gaps in relative energies for the three (Zn–Cd)₅ iso-

Table 1 Comparison of single point energies for the three low-lying isomers of (Zn–Cd)₅.

Method	5a	5b	5c
CCSD(T)	0	0.08	0.13
PBE0	0	0.10	0.15
TPSS	0	0.14	0.21
TPSSH	0	0.13	0.18
BP86	0	0.12	0.18
M06	0	0.10	0.16

Other energies are relative to 5a, and the units are eV

mers optimized using the PBE0 functional are in excellent agreement with those obtained from the CCSD(T) method. Furthermore, the energetic sequences of the three isomers computed using the PBE0 functional are also consistent with those obtained using other functionals.

The Fig. 1 plots the GM structures and isomers of Zn–Cd clusters, only involving singlet states, which are more stable by > 1.0 eV than the corresponding high-spin states. Their point groups of symmetry are also given, and relative energies are arranged in order from low to high. The partial isomers within 0.5 eV of the GM structures in energies are given because there is a mass of isomers per cluster. The true local minima of potential energy surfaces at the same theory level are confirmed by checking vibrational frequency.

The Zn–Cd dimer shows a linear configuration. The (Zn–Cd)₂ is found to have only a triangular pyramid with the C_{2v} symmetry, and other calculated structures eventually fail to converge. The GM 3a of (Zn–Cd)₃ isomers is in C_{2v} symmetry and it presents a spherical compact structure linked to one separate Cd atom, where three Zn atoms and three Cd atoms are in two planes perpendicular to each other. The metastable isomer 3b with C_s symmetry is only 0.03 eV

higher in energy. The isomers of (Zn–Cd)₄ have irregular structures, and the 4a with C_s symmetry is most stable. The GM 5a for (Zn–Cd)₅ is a square antiprism with C_s symmetry, which can be obtained by capping one Cd atom on a tricapped trigonal prism. The 5a, 5b and 5c have the same structural frameworks, but the arrangements of Zn and Cd atoms are different. The isomers of (Zn–Cd)₆ have compact structures, and the GM 6a with C_s symmetry is based on the growth of 5a. The GM 7a with C_s symmetry adopts a prolate motif, which can be built from the 5a with Cd₄ linked to the spherical cage. The 7b and 7c also have the same structural frameworks. The GM 8a can be seen as an integration of two 5a structures. The isomers of (Zn–Cd)₉ have compact structures, and the GM 9a is in the C_s symmetry. Furthermore, the presences of the same structural skeleton but different atomic arrangement in the Zn–Cd isomers further indicate that the search strategy we used can deal well with the HOMOTOP problem in alloy clusters.

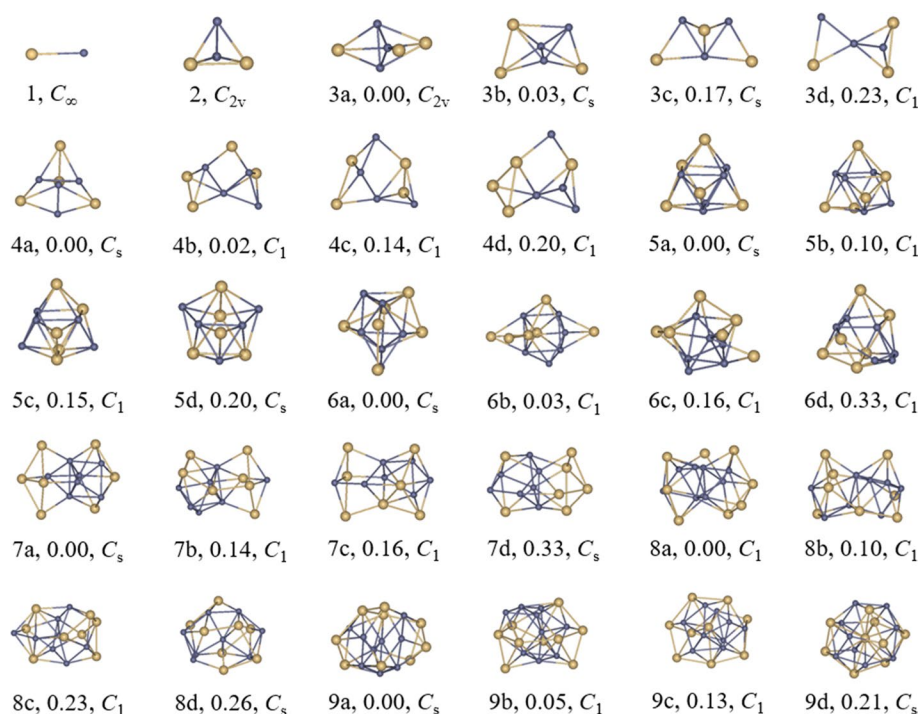
Overall, the (Zn–Cd)_n (n = 1–9) clusters show a great diversity and flexibility in geometric structures, which adopt compact structures with cluster size n. For n ≥ 2, GM structures of Zn–Cd clusters are more inclined to 3D configurations with singlet states. The Zn and Cd atoms do not mix in the Zn–Cd clusters, and they tend to be centrally distributed, respectively. Moreover, Cd atoms prefer to be located on the surfaces of the cluster structures, thus coating Zn atoms that are for the kernel growths.

The Stability of (Zn–Cd)_n (n = 1–9) Clusters

The relative stability of (Zn–Cd)_n (n = 1–9) clusters are compared by the binding energy (E_b) and the second difference in energy (Δ₂E), which illustrate the relationship between the stability and compositions of different sizes. As the zero of energy for the Cd and Zn atoms are different, a good binding energy would be to use E_b = [nE(Zn–Cd) – E(Zn–Cd)_n]/n. This binding energy vs n^(–1/3) is also plotted to get an estimate of the cohesive energy relative to the diatomic Zn–Cd. The formula of Δ₂E is defined as E(Zn–Cd)_{n+1} + E(Zn–Cd)_{n–1} – 2E(Zn–Cd)_n.

Fig. 2 plots of the E_b curve with GM structures and Δ₂E curve, where these quantities as two functions of the considered (Zn–Cd)_n (n = 1–9) clusters with the number n. The E_b curve as shown in Fig. 2a of the Zn–Cd clusters has an approximately monotonically rising trend, and the curve appears two local maximums at n = 2 and 5, respectively. According to the definition of the E_b equation, we can conclude that the (Zn–Cd)₂ and (Zn–Cd)₅ clusters have higher stability than that of their neighbors. The reasons may be that these two clusters have electronic shell closures. The fitted straight line of the E_b vs n^(–1/3) is plotted in the Fig. 2b to estimate the cohesive energy of the bulk with respect to

Fig. 1 Optimized structures of $(\text{Zn-Cd})_n$ ($n = 1-9$) at the PBE0/Def2-SVP level. The labels are energy (eV) relative to the GM one and symmetry. Cd-yellow, Zn-gray (Color figure online)



the ZnCd dimer. From the Fig. 2c, we can intuitively see that the $\Delta_2 E$ curve of Zn-Cd clusters does not exhibit an odd-even oscillation behavior commonly seen in alloy clusters. But distinct peaks of it also appear at $n = 2$ and 5. This result also further verifies that the $(\text{Zn-Cd})_2$ and $(\text{Zn-Cd})_5$ clusters are very salient on the E_b curve. Moreover, here it is worth mentioning that geometric closure is an important factor for stability of $(\text{Zn-Cd})_2$ and $(\text{Zn-Cd})_5$ clusters.

In order to further investigate the thermal stability of Zn-Cd clusters, we implement the ab initio molecular dynamics simulations. The modeling process, the structures were placed in a $15 \times 15 \times 15 \text{ \AA}$ box to avoid interactions between the individual clusters. We selected the 300 K, 500 K and 700 K as initial temperatures for AIMD simulations, respectively. The duration time of each temperature is 10 ps, and the time step is set to 1.0 fs. Moreover, we extracted structure snapshots every 20 fs to observe the structural changes in detail. The energy fluctuations with the time step of AIMD simulations are plotted in Fig. 3, and we found that the geometric constructions of $(\text{Zn-Cd})_2$ and $(\text{Zn-Cd})_5$ can keep integrality with only minor disturbances of individual atoms at a temperature of 700 K, suggesting that they have good thermal stability at high temperature environments.

Superatom and Electronic Structures of the $(\text{Zn-Cd})_2$ and $(\text{Zn-Cd})_5$ Clusters

Searching stable structures of metal clusters is one of rapidly developing frontier fields, e.g. superatom clusters [48–50].

We know that the stability of them is codetermined by both geometries and electronic characteristics. It is generally acknowledged that when electron shells are closed, the size-dependent stability characteristics begin to appear in the cluster series. Here, the $(\text{Zn-Cd})_2$ and $(\text{Zn-Cd})_5$ clusters have higher stability than that of their neighbors, and they also have good thermal stability at high temperatures. Since the geometric structures and the number of 8/20 valence electrons all fit the jellium model, do filling situations of their valence electrons also satisfy as well?

As transition metals, Zn has a valence electron configuration of $3d^{10}4s^2$, and Cd has a valence electron configuration of $4d^{10}5s^2$, in which $3d^{10}$ electrons of Zn and $4d^{10}$ electrons of Cd are usually localized as lone pairs. What is the electronic structure of the hybrid cluster formed by them? In order to clarify the 8/20 valence electrons filling details of $(\text{Zn-Cd})_2$ and $(\text{Zn-Cd})_5$ clusters, we calculate their canonical molecular orbitals (MOs) at the PBE0/Def2-SVP level. Fig. 4 shows the MOs of the $(\text{Zn-Cd})_2$ and $(\text{Zn-Cd})_5$ clusters, from which we can easily identify one S-type and three P-type superatomic orbitals for the $(\text{Zn-Cd})_2$, as well one 1S-type, three 1P-type, five 1D-type and a 2S-type superatomic orbitals for the $(\text{Zn-Cd})_5$, respectively. In brief, the 8/20 valence electrons of the $(\text{Zn-Cd})_2$ and $(\text{Zn-Cd})_5$ clusters fill the superatomic shells resulting in electronic configurations of $1S^2 1P^6 / 1S^2 1P^6 1D^{10} 2S^2$, respectively, which are also why they all are singlet states. The adaptive natural density partitioning (AdNDP) and electronic localization function (ELF) are further implemented, and the results in the Fig. S1 show very obvious electron delocalized

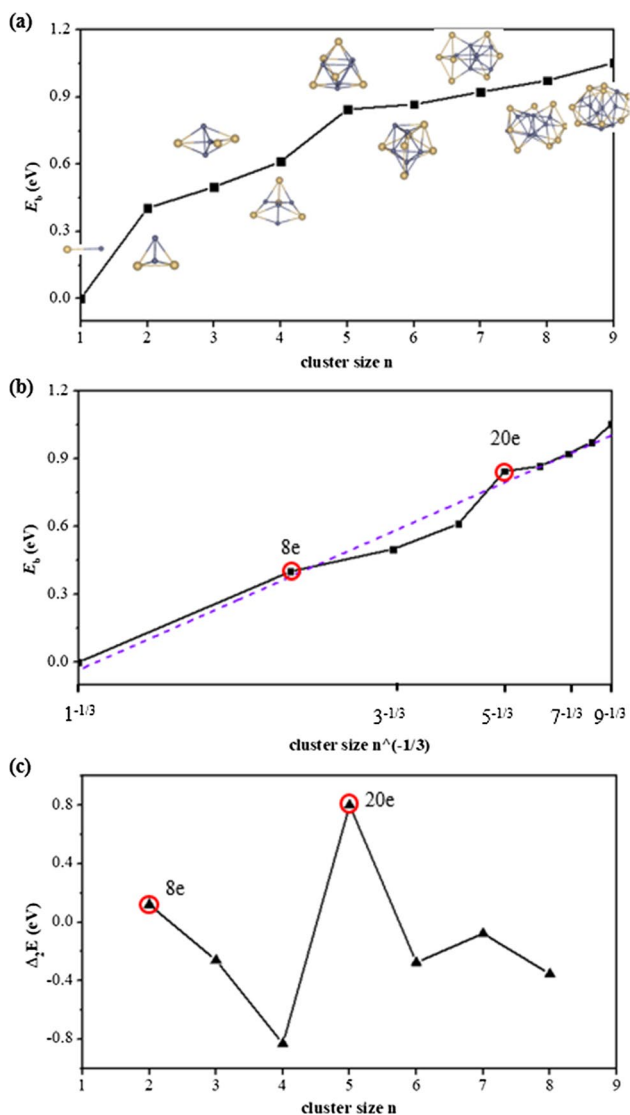


Fig. 2 **a** The binding energy (E_b), **b** the fitted straight line of E_b vs $n^{-1/3}$, and **c** the second difference in energy ($\Delta_2 E$) for (Zn–Cd) $_n$ ($n = 1$ –9) clusters

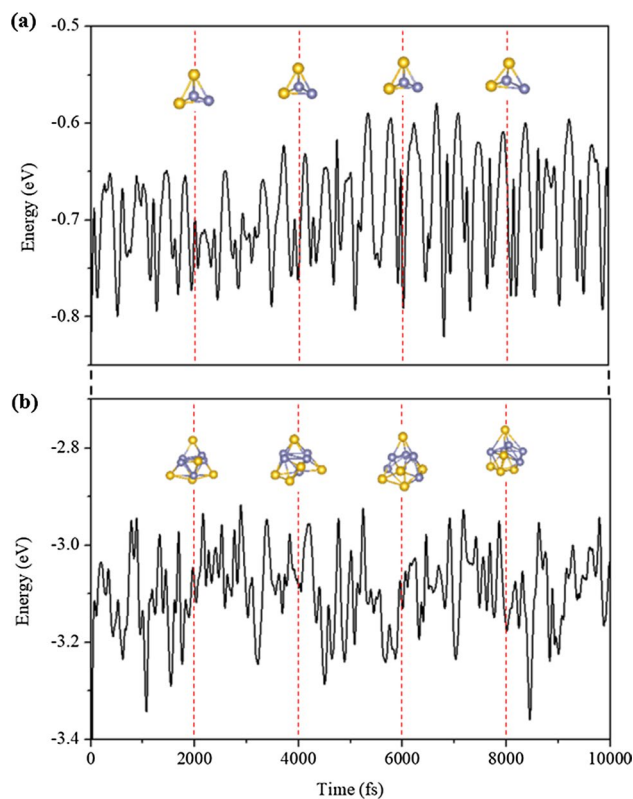


Fig. 3 AIMD simulations of the **a** (Zn–Cd) $_2$ and **b** (Zn–Cd) $_5$ cluster energy trajectories with the time step at 700 K

characteristics throughout the whole spaces [45, 51]. Thus, the (Zn–Cd) $_2$ and (Zn–Cd) $_5$ clusters in the geometric and electronic structures all conform to the jellium model, and they can be thought of as stable 8/20e superatoms.

The above observations are further analyzed by the density of states. From the Fig. 4, we clearly find that the intensity and distributions of the DOS curves are in very good agreement. The total DOS curves of the (Zn–Cd) $_2$ and (Zn–Cd) $_5$ clusters are almost entirely derived from the superposition of the partial DOS of Zn and Cd atoms, both of which have joint contributions. Combining the energy range of superatomic orbitals ($1S^21P^6/1S^21P^61D^{10}2S^2$), they can be further considered that the total DOS of the (Zn–Cd) $_2$ and (Zn–Cd) $_5$ clusters come from contributions of 8/20 s electrons of Zn and Cd atoms. We can see that the contributions of s electrons are the maximum, while the contributions of d electrons are the minimum, and that of p electrons are in between d electrons and s electrons. These are also exactly agreement with the above MOs orbitals analysis results. We also compare with the DOS curves of their adjacent clusters, and the results are shown in the Fig. S2.

The (Zn–Cd) $_2$ and (Zn–Cd) $_5$ clusters exhibit non-spherical shapes. In fact, the grouping of electronic orbitals is closely related to the geometry of the cluster. An illustrative example of the relationship between electronic and

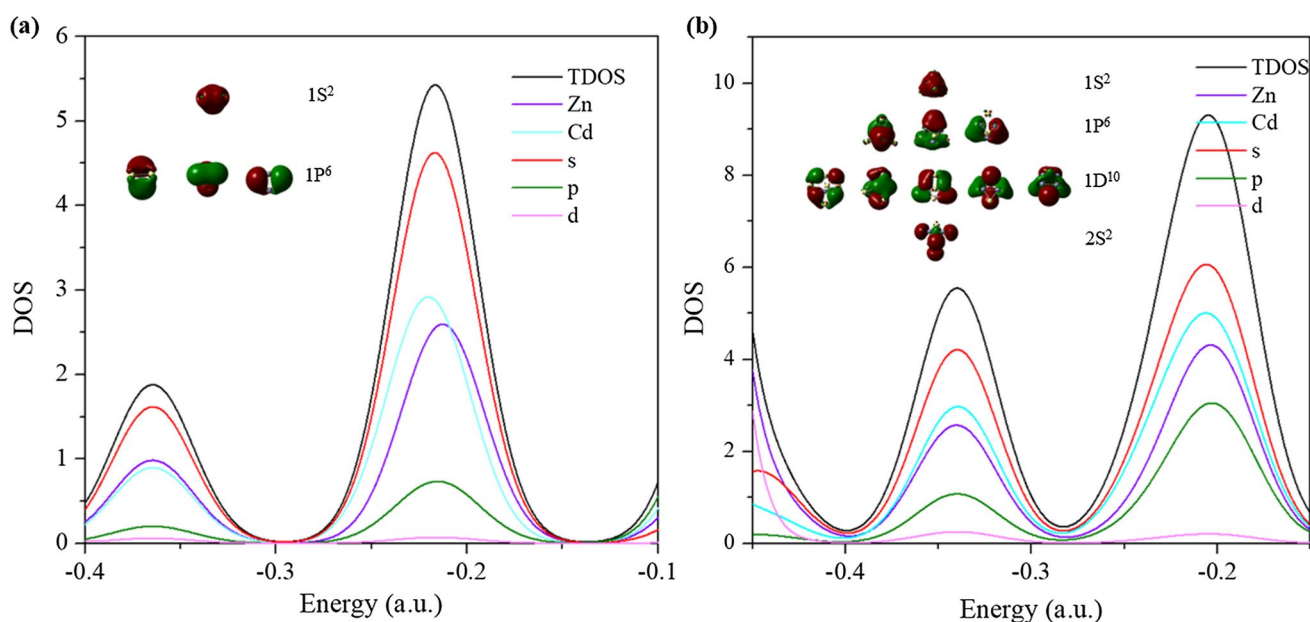


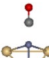



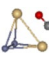
Fig. 4 The molecular orbital diagrams and the density of states of **a** $(\text{Zn-Cd})_2$ and **b** $(\text{Zn-Cd})_5$ clusters

geometric structure is that geometrical distortions can lead to the splitting of electronic shells into subshells with a large HOMO–LUMO gap granting the cluster the stability associated with a magic species. Unlike individual atoms, a cluster with a partially filled subshell can stabilize itself either by undergoing a Jahn–Teller distortion to form a singlet state with a gap within a subshell [30, 52]. As a result, the structures of these two superatoms deviate slightly from the spherical jellium model due to the Jahn–Teller Effect.

Adsorption Characters of the $(\text{Zn-Cd})_2$ Cluster

Metal clusters with two different atoms possess uneven charge distributions over all geometrical surfaces, resulting in the formations of reactive sites that can enable the substances to activate. Since small-sized Au clusters are reported to have fascinatingly catalytic activity for the CO oxidation reaction, revealing new mechanisms of catalytic/adsorption reactions on surfaces of alloy clusters is received high-level concerns, due to CO being involved in several energy-related and environmental processes [53–55]. For example, Gao et al. reported that the $\text{Au}_{43}\text{Cu}_{12}$ icosahedron has prospectively catalytic activities for CO oxidation and selectivity for styrene oxidation [56]. However, there are too many possible reactive sites of the cluster surfaces for the heterogeneous catalysis to consider every possibility. Based on the configurations by our optimization computations, we focus on a simple adsorption pattern of the $(\text{Zn-Cd})_2\text{-CO}$ as a typical example to reveal catalytic potential of Zn–Cd clusters.

Table 2 Relative energies (ΔE), bond length (r) and vibrational frequency (ν) of $(\text{Zn-Cd})_2\text{-CO}$.

Structures	ΔE (eV)	$r_{(\text{C-O})}$ (Å)	$\nu_{(\text{C-O})}$ (cm^{-1})
	0.00	1.130	2244.03
 (iso1)	0.03	1.129	2251.47
 (iso2)	0.07	1.128	2271.05
 (iso3)	0.15	1.128	2268.80
 (iso4)			

We considered many initial adsorption structures of $(\text{Zn-Cd})_2$ with one CO. The CO is placed in the top, hollow and bridge sites to consider the effectiveness of optimal adsorptions. However, many calculated initial structures either have imaginary frequencies or do not converge to local minima. All isomers of the $(\text{Zn-Cd})_2\text{-CO}$ clusters are finally obtained at the theoretical level of PBE/Def2-SVP, and frequencies of vibrations are also checked after geometrical optimizations. Table 2 give isomer structures of the $(\text{Zn-Cd})_2\text{-CO}$, and only the four stable ones are finally obtained which relative energies (ΔE) of them are arranged in order from low to high. After one CO are adsorbed on different positions of the surface of $(\text{Zn-Cd})_2$, we found that C–O bond length and vibrational frequency did not change significantly compared with the free CO. Due to that the $(\text{Zn-Cd})_2$ has a good stability in the geometric and electronic

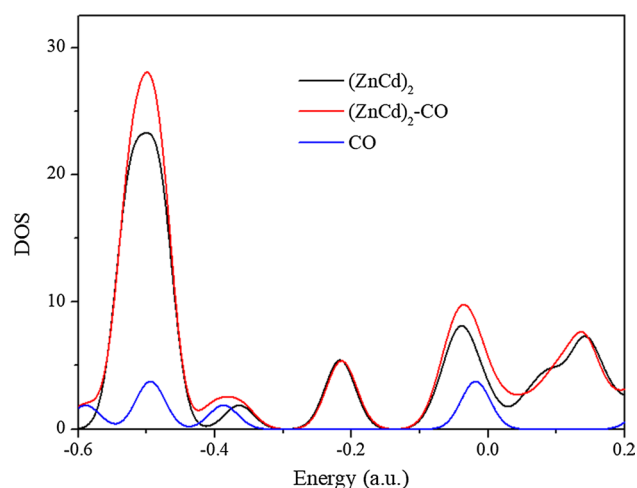

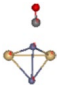


Fig. 5 The density of states of the $(\text{ZnCd})_2$, $(\text{ZnCd})_2\text{-CO}$ and CO.

Table 3 NPA charge of $(\text{Zn-Cd})_2$ and $(\text{Zn-Cd})_2\text{-CO}$.

Atoms	Cluster and NPA charge	Cluster and NPA charge
		
Zn1	0.19	0.19
Zn2	0.19	0.21
Cd3	-0.19	-0.19
Cd4	-0.19	-0.19

structures, it is favorable for CO in the form of molecule to adsorb on the cluster (physical absorption), resulting in the unbroken C–O bond.

To gain a new understanding of the electronic effects of one CO molecule attached to the $(\text{Zn-Cd})_2$ cluster, we analyzed its density of states. The DOS curves for the CO molecule and $(\text{Zn-Cd})_2$ cluster before and after interactions are presented in Fig. 5. It is found that the DOS curve of the $(\text{Zn-Cd})_2\text{-CO}$ is almost entirely derived from $(\text{Zn-Cd})_2$ cluster, where the intensity and distributions of the curve are in very good agreement, while the contributions of CO at this time are almost negligible. The result shows that the electronic structure of $(\text{Zn-Cd})_2$ cluster has excellent stability, which also confirms the physical absorption of CO. The NPA charge of $(\text{Zn-Cd})_2$ and $(\text{Zn-Cd})_2\text{-CO}$ were calculated to further analyze charge transfers between the metal cluster and CO fragment. As shown in the Table 3, the adsorption only causes very slight changes in the NPA charges of Zn2 atom, and charge of other metal atoms didn't change. In brief, the $(\text{Zn-Cd})_2$ cluster loses a tiny fraction of its charge, and these are transferred to the CO molecule, which also is consistent with the above DOS analysis results.

Conclusions

In summary, geometric structures of $(\text{Zn-Cd})_n$ ($n = 1-9$) clusters are globally searched by using the unbiasedly GA-DFT methods. The configuration features, stability and electronic structures of them are emphatically analyzed. For $n \geq 2$, GM structures of Zn–Cd clusters are more inclined to 3D configurations with singlet states. The Zn and Cd atoms do not mix in the Zn–Cd clusters, and they tend to be centrally distributed, respectively. Moreover, Cd atoms prefer to be located on the surfaces of the cluster structures, thus coating Zn atoms that are for the kernel growths. The E_b and Δ_2E results analysis show that the $(\text{Zn-Cd})_2$ and $(\text{Zn-Cd})_5$ clusters have higher stability than that of their neighbors. The AIMD simulations show that they still have a good thermal stability at 700K. The molecular orbitals and DOS reveal that the 8/20 valence electrons of the $(\text{Zn-Cd})_2$ and $(\text{Zn-Cd})_5$ clusters fill the superatomic shells resulting in electronic configurations of $1S^21P^6/1S^21P^61D^{10}2S^2$, respectively, where almost all of them come from the combined contributions of Zn and Cd atoms. Moreover, we considered many initial adsorption structures of $(\text{Zn-Cd})_2$ with one CO, and only the four stable isomers are finally obtained. Due to that the $(\text{Zn-Cd})_2$ has a good stability in the geometric and electronic structures, it is favorable for CO in the form of molecule to adsorb on the cluster (physical absorption), resulting in the unbroken C–O bond.

Supplementary Information The online version contains supplementary material available at <https://doi.org/10.1007/s10876-023-02472-1>.

Author Contributions YM: Methodology, Software, Writing—original draft. QL: Writing - review & editing. LC: Supervision. All authors reviewed the manuscript

Funding This work is supported by the Horizontal Cooperation Project of Huainan Normal University (2022HX47) and the Key Project of Scientific Research Foundation of Anhui Province Education Department (KJ2021A0962). The calculations were carried out at the High-Performance Computing Center of Anhui University.

Data Availability The data presented in this study are available upon request from the corresponding authors.

Declarations

Conflict of interest The authors state that there is no conflict of interest.

Ethical Approval Not applicable.

References

- O. Schulte and W. B. Holzapfel (1996). *Phys. Rev. B* **53**, 569.
- R. Ferrando, J. Jellinek, and R. L. Johnston (2008). *Chem. Rev.* **108**, 845.

3. R. Bohl and V. Hildebrandt (1957). *J. Am. Chem. Soc.* **79**, 2711.
4. F. Meydani, B. Saatçi, M. Gündüz, and M. Özdemir (2007). *Surf. Sci.* **601**, 2171.
5. O. Awe and A. Azeez (2017). *Appl. Phys. A* **123**, 1.
6. R. Hatz, V. Hanninen, and L. Halonen (2014). *J. Phys. Chem. A* **118**, 12274.
7. L. Amirouche and Ş Erkoç (2004). *Phys. Stat. Sol.* **241**, 292.
8. L. Amirouche and Ş Erkoç (2005). *J. Cryst. Growth* **275**.
9. H. Limbu and G. Adhikari (2020). *Int. J. Phys.* **8**, 81.
10. C. Zanvetto and J. Marques (2014). *Chem. Phys. Lett.* **608**, 373.
11. Y. Wang, X. Chen, and C. Chen (2021). *Inorg. Chem. Commun.* **134**.
12. S. J. McCormack and A. Navrotsky (2021). *Acta Mater.* **202**, 1.
13. O. Akinlade and O. Awe (2006). *Int. J. Mater. Res.* **97**, 377.
14. A. Pola, M. Tocci, and F. E. Goodwin (2020). *Metals* **10**, 253.
15. P. Fima and R. Novakovic (2018). *Philos. Mag.* **98**, 1608.
16. O. Fornaro and H. A. Palacio (2006). *Scripta Mater.* **54**, 2149.
17. B. Saatçi, M. Ari, M. Gündüz, F. Meydani, M. Bozoklu, and S. Durmuş (2006). *J. Phys-Condens Mat.* **18**, 10643.
18. R. Koirala, B. Singh, I. Jha, and D. Adhikari (2013). *J. Mol. Liq.* **179**, 60.
19. G. Shrestha and I. Koirala (2021). *J. Nepal Phys. Soc.* **7**, 17.
20. H. S. Oh, S. J. Kim, K. Odbadrakh, W. H. Ryu, K. N. Yoon, S. Mu, F. Körmann, Y. Ikeda, C. C. Tasan, and D. Raabe (2019). *Nat. Commun.* **10**, 1.
21. A. Smekhova, A. Kuzmin, K. Siemensmeyer, C. Luo, K. Chen, F. Radu, E. Weschke, U. Reinholz, A. G. Buzanich, and K. V. Yusenko (2022). *Nano Res.* **15**, 4845.
22. G. L. Hart, T. Mueller, C. Toher, and S. Curtarolo (2021). *Nat. Rev. Mater.* **6**, 730.
23. S. Sarkar, O. Eriksson, D. Sarma, and I. Di Marco (2022). *Phys. Rev. B* **105**.
24. A. Lebon, A. Aguado, and A. Vega (2015). *Phys. Chem. Chem. Phys.* **17**, 28033.
25. R. B. Adamson, C. E. Coleman, and M. Griffiths (2019). *J. Nucl. Mater.* **521**, 167.
26. V. Roche, G. Koga, T. Matias, C. Kiminami, C. Bolfarini, W. Botta, R. Nogueira, and A. J. Junior (2019). *J. Alloys Compd.* **774**, 168.
27. C. Yan, K. Sun, J. Huang, S. Johnston, F. Liu, B. P. Veetil, K. Sun, A. Pu, F. Zhou, and J. A. Stride (2017). *ACS Energy Lett.* **2**, 930.
28. L. Amirouche and Ş Erkoç (2003). *Int. J. Mod. Phys. C* **14**, 905.
29. L. Amirouche and Ş Erkoç (2003). *Phys. Rev. A* **68**.
30. A. C. Reber and S. N. Khanna (2017). *Acc. Chem. Res.* **50**, 255.
31. J. U. Reveles, P. A. Clayborne, A. C. Reber, S. N. Khanna, K. Pradhan, P. Sen, and M. R. Pederson (2009). *Nature Chem.* **1**, 310.
32. P. Jena and Q. Sun (2018). *Chem. Rev.* **118**, 5755.
33. D. E. Bergeron, A. W. Castleman Jr., T. Morisato, and S. N. Khanna (2004). *Science* **304**, 84.
34. S. Heiles, A. J. Logsdail, R. Schäfer, and R. L. Johnston (2012). *Nanoscale* **4**, 1109.
35. S. G. Neogi and P. Chaudhury (2012). *J. Comput. Chem.* **33**, 629.
36. S. Ganguly and P. Neogi (2014). *J. Comput. Chem.* **35**, 51.
37. M. Aslan, J. B. Davis, and R. L. Johnston (2016). *Phys. Chem. Chem. Phys.* **18**, 6676.
38. Q. Liu, P. Fan, Y. Hu, F. Wang, and L. Cheng (2021). *Phys. Chem. Chem. Phys.* **23**, 10946.
39. Z. Tian and L. Cheng (2017). *J. Phys. Chem. C* **121**, 20458.
40. J. Zhao, Q. Du, S. Zhou, and V. Kumar (2020). *Chem. Rev.* **120**, 9021.
41. J. P. Perdew, K. Burke, and M. Phys (1996). *Rev. Lett.* **77**, 3865.
42. F. Weigend and R. Ahlrichs (2005). *Phys. Chem. Chem. Phys.* **7**, 3297.
43. M. Frisch, G. Trucks, H. Schlegel, G. Scuseria, M. Robb, J. Cheeseman, G. Scalmani, V. Barone, B. Mennucci, and G. Petersson, *Gaussian 09; Revision B. 01* (Gaussian Inc, Wallingford, 2010).
44. U. Varetto, *MOLEKEL version 5.4.0.8* (Swiss National Supercomputing Centre, Manno, Switzerland, 2009)
45. T. Lu and F. Chen (2012). *J. Comput. Chem.* **33**, 580.
46. J. Hafner (2008). *J. Comput. Chem.* **29**, 2044.
47. M. E. Tuckerman, P. J. Ungar, T. Von Rosenvinge, and M. L. Klein (1996). *J. Phys. Chem.* **100**, 12878.
48. B. Yin and Z. Luo (2021). *Coordin. Chem. Rev.* **429**.
49. H. Häkkinen (2008). *Chem. Soc. Rev.* **37**, 1847.
50. E. A. Doud, A. Voevodin, T. J. Hochuli, A. M. Champsaur, C. Nuckolls, and X. Roy (2020). *Nat. Rev. Mater.* **5**, 371.
51. N. V. Tkachenko and A. I. Boldyrev (2019). *Phys. Chem. Chem. Phys.* **21**, 9590.
52. M. A. Tofanelli, K. Salorinne, T. W. Ni, S. Malola, B. Newell, B. Phillips, H. Häkkinen, and C. J. Ackerson (2016). *Chem. Sci.* **7**, 1882.
53. Z. Luo, A. Castleman Jr., and S. N. Khanna (2016). *Chem. Rev.* **116**, 14456.
54. W. T. Wallace and R. L. Whetten (2002). *J. Am. Chem. Soc.* **124**, 7499.
55. Y. Gao, N. Shao, Y. Pei, Z. Chen, and X. C. Zeng (2011). *ACS Nano* **5**, 7818.
56. Y. Gao, N. Shao, Y. Pei, and X. C. Zeng (2010). *Nano Lett.* **10**, 1055.

Publisher's Note Springer Nature remains neutral with regard to jurisdictional claims in published maps and institutional affiliations.

Springer Nature or its licensor (e.g. a society or other partner) holds exclusive rights to this article under a publishing agreement with the author(s) or other rightsholder(s); author self-archiving of the accepted manuscript version of this article is solely governed by the terms of such publishing agreement and applicable law.